Sensing and Bio-Sensing Research 41 (2023) 100572

Contents lists available at ScienceDirect

Sensing and Bio-Sensing Research

journal homepage: www.elsevier.com/locate/sbsr

Design of Quasi-Shaped spectroscopy based optical sensor for the detection of alcohol

Md. Selim Hossain [a], Rakib Hossen [b], Md. Abul Ala Walid [c], Syada Tasmia Alvi [d], Md. Al-Amin [e], Shuvo Sen [f,*], Mir Mohammad Azad [g]

[a] Department of Electronics and Communication Engineering (ECE), Hajee Mohammad Danesh Science and Technology University (HSTU), Dinajpur 5200, Bangladesh
[b] Department of Educational Technology (ET), Bangabandhu Sheikh Mujibur Rahman Digital University, Bangladesh Kaliakoir, Gazipur 1750, Bangladesh
[c] Department of Computer Science and Engineering, Khulna University of Engineering and Technology (KUET), Khulna 9203, Bangladesh
[d] Department of Computer Science and Engineering, Daffodil International University, Dhaka, Bangladesh
[e] Department of Electrical and Electronic Engineering (EEE), Daffodil International University, Dhaka, Bangladesh
[f] Department of Information and Communication Technology (ICT), Mawlana Bhashani Science and Technology University (MBSTU), Santosh, Tangail 1902, Bangladesh
[g] Department of Computer Science and Engineering, Independent Researcher, Dhaka, Bangladesh

ARTICLE INFO

Keywords:
Quasi-shaped PCF
Optical sensor
EML
Spectroscopy
Detection
Alcohol
Etc.

ABSTRACT

In this research, an entirely novel optical sensor for alcohol detection based on quasi-shaped spectroscopy is offered. A quasi shape with a tightly bonded structure in the cladding region and a hexahedron core region makes up the recommended design, which has a remarkable sensitivity of about 91.35%, 92.55%, and 90.40%and low confinement losses (CLs) of 5.44×10^{-08} dB/m, 6.75×10^{-08} dB/m, and 5.85×10^{-08} dB/m for detecting alcohol like ethanol ($n = 1.354$), butanol ($n = 1.3993$), and propanol($n = 1.384$), at 1 THz. The numerical aperture, the effective area, and the V-parameter have all been identified and assessed. The 0.8THz to 3 THz operational wavelength range is stated. In the COMSOL Multiphysics (Version 5.6) environment, the properties of these suggested alcohol sensors are numerically examined utilizing the FEM (finite element method) with full vectors. In contrast to other efforts, the proposed sensor, which consists of a quasi-lattice PCF with a perfectly matched layer (PML) of a circular air hole shape and TOPAS as the background material, aims to improve sensitivity response. The proposed sensor might be crucial in the alcohol detection process due to its superior sensitivity response, a single mode of operation across the entire operational terahertz range, and shallow confinement loss. So, this PCF can proficiently be pragmatic in many biological sensing and other THz technology domains.

1. Introduction

Recently, the exploration of exploring and development of the fiber made with photonic crystals' optical characteristics. Numerous nonlinear optical systems, fiber lasers, spectroscopy, medical and biotechnology uses, applications for the environment, test for drugs for pharmaceuticals, and sensors that are acute are just a few of the numerous potential benefits of fiber optics [1–4]. This is due to its optical qualities. Chemical sensing applications are now in favor of PCF in the THz regime. The primary factor influencing this field's appeal is the ability to modify the geometrical parameters to optimize the sensing characteristics. Light-matter interaction is increased, and new sensing applications are made possible by the hollow core PCF's larger analyte volume in the core area compared to that porous core. Various beverages include ethanol, an intoxicating substance that can lead to coma, death, addiction, and other adverse effects. The presence of ethanol (ethyl alcohol) in beverages is therefore essential. For identifying alcoholic components in liquid samples, many researchers have recently developed various PCF geometries. A hybrid photonic crystal fiber for chemical sensing was created by S. Asaduzzaman and colleagues. For ethanol, this design was claimed to have a sensitivity of 49.17% [5]. With minimal loss and 59% increased sensitivity, Arif et al. suggested hexagonal-constructed PCF as a sensor for liquid detection [6]. They achieved higher sensitivity using the design suggested by S. Asaduzzaman et al. Taking this into account, J. Sultana et al. showed a TOPAS-based PCF for ethanol sensing that reached 68.87% of sensitivity

* Corresponding author.
E-mail address: shuvombstu.it12009@gmail.com (S. Sen).

https://doi.org/10.1016/j.sbsr.2023.100572
Received 30 April 2023; Received in revised form 8 July 2023; Accepted 27 July 2023
Available online 29 July 2023

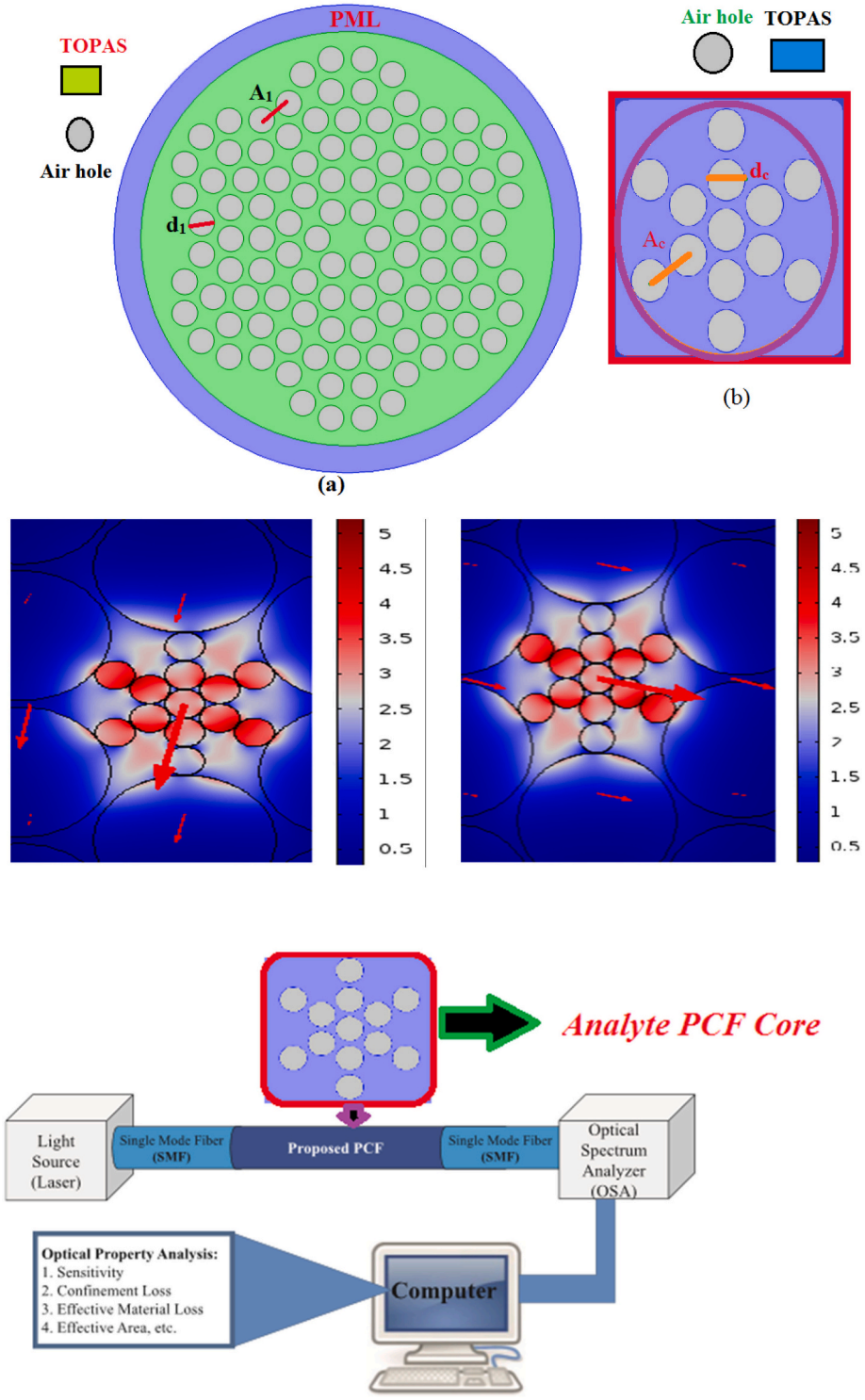

Fig. 1. Pictured are (a) the quasi-shaped cladding (b) the core area of the hexahedron (c) and the mode field distributions for both x and polarization of 1 THz.

along with 7.79 × 10^{-12} cm^{-1} loss of confinement at a frequency of 1 THz [7]. B.K. Paul et al. developed a crystal photonic fiber with circular air holes, which had a relative sensitivity of 64.19% and a confinement loss of 2.07 × 10^{-5} dB/m over a length of 1.48 m [8]. H. Ademgil and colleagues suggested a sensor built on a PCF that has lower confinement losses and can be used for detecting liquid analytes. Only 26% of the proposed PCF architecture was sensitive. In the previous review of articles in [5–8], we see that the relative sensitivity level is low. As a result, this low amount of relative sensitivity is not easily to detect the alcohols in the biomedical or industrial areas. So, according to the previous work, we find a great opportunity to design a new photonic crystal fiber with the high relative sensitivity and the low confinement loss in the terahertz (THz) waveguide for alcohols sensing applications.

We offer an alcohol-detection THz sensor based on photonic crystal fiber that considers the impacts of alcoholic beverages. The described alcohol sensor has an extremely low confinement loss and a sensitivity of over 90%. Additionally, it outperformed other recently published designs in the literature [5–9], revealing 1.1 × 10^{-7} m^2 of effective area

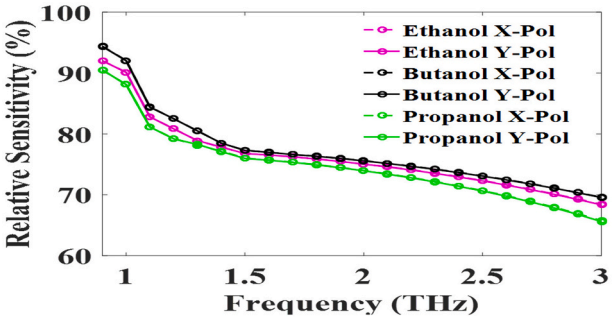

Fig. 2. Analysis of the sensitivity as well as the frequency of three compounds for both at optimal conditions.

and (0.008–0.018) cm^{-1} of effective material loss for frequencies between (0.8 and 3 THz). In this study, we simplified the geometrical form of the PCF while increasing relative sensitivity in biochemical recognition and lowering production simplification. Regarding effective material loss and minimal containment loss, we measured how big the core is and how far apart the air holes are and changed those. The resulting effective wide area of the proposed Quasi-Shaped Spectroscopy based PCF sensor allows for the injection of a large volume of the analyses. With maximum relative sensitivity of 91.35%, 92.55%, and 90.40%and low confinement losses (CLs) of 5.44×10^{-08}, 6.75×10^{-08} dB/m, and 5.85×10^{-08} dB/m for detecting chemicals like ethanol, butanol, and propanol at 1 THz, our proposed quasi-shaped PCF stands out among previous publications [25–31].

2. Design methodology

The configuration of PCF, which has a hexahedron-shaped core area, a quasi-shaped cladding, and field mode supplies for x and y polarization at a frequency of 1 THz, is shown in Fig. 1. In the cladding area, the diameter and pitch are defined with the parameters of d_1 and Λ_1 according to the proper design procedure. In the contrary, d_c and Λ_c parameters are indicated by the hexahedron-shaped of core area. There are three alcohols like ethanol (n = 1.354), butanol (n = 1.3993), and propanol(n = 1.384), filled up in the core area with their refractive index values. On the other hand, TOPAS is used as a background material and help to obtain the high relative sensitivity and low confinement loss. So, we can say clearly that our fiber is designed with perfectly matched layers (PML) and the finite element method (FEM) based COMSOL Multiphysics software tool to achieve guiding properties such as the relative sensitivity, confinement loss, effective area, and effective mode index according to the terahertz frequency wave range from 0.80 to 3.0 THz. Here, the PML (boundary condition) of thickness is indicated by the 10% of the maximum fiber diameter and optimized design parameters for core diameter (d_c) = 80 μm, core pitch (Λ_c) = 82 μm, five layers of cladding diameter d1 = d2 = d3 = d4 = d5 = 300 μm and five layers of cladding pitch such as $\Lambda_1 = \Lambda_2 = \Lambda_3 = \Lambda_4 = \Lambda_5$ = 360 μm,

In Fig. 1(c), we visualize that the full light passes through the core areas strongly for (a) x-polarization and (b) y-polarization modes. As a result, we get the high relative sensitivity and low confinement loss for both polarizations of modes at the operating region of 1 THz.

In Fig. 1(d), the light laser is passed through the analytic PCF core, and the optical spectrum analyzer **(OSA)** will provide data to the computer to analyze the optical properties like effective area, RS, CL, and effective mode index of the injected alcohols. Then the computer will represent data numerically and graphically procedure.

Figure 1(d): Representation of the working procedure of the proposed PCF model [16].

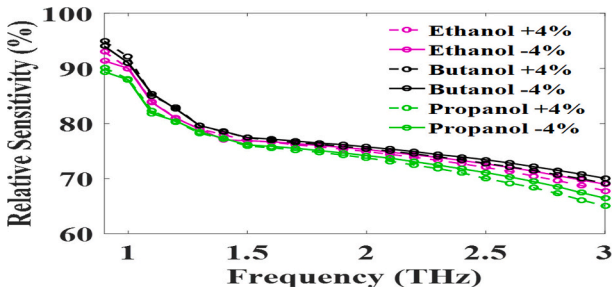

Fig. 3. For both polarizations at ±4% Variation Parameters, sensitivity analysis and the frequency of three compounds were performed.

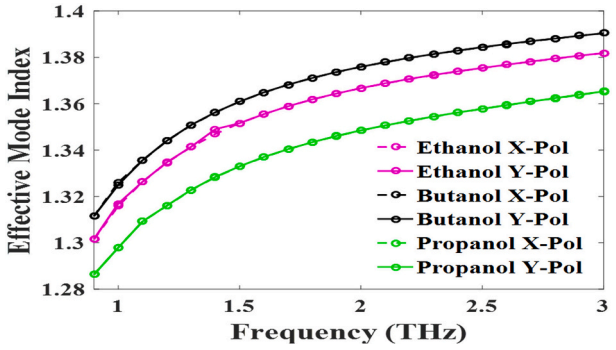

Fig. 4. The EMI pertaining to the three-fold frequency compounds for equally polarized under ideal conditions.

3. Numerical analysis, discussion, and results analysis

The consciousness of the fact that the method chooses the relative sensitivity [18]:

$$R = \frac{n_a}{n_{eff}} \times P \tag{1}$$

$N_{eff,}$ the analyte's effective guided mode index, was calculated using the FEM approach in relation to various frequencies during simulation. Figs. 2 and 3 shows the corresponding frequency as well as the mode index value for both the x- and y-modes. P stands for a measure of power factor, and is the mathematical notation for it [19]:

$$P = \frac{[\int Re(Ex, Hy, Ey, Hx)dxdy]^1}{[\int Re(Ex, Hy, Ey, Hx)dxdy^1} x100 \tag{2}$$

The symbols Hx and Hy are used to indicate the magnitude of the horizontal x and y directions' magnetic fields. On the other hand, the symbols Ex and Ey refer to the electric field strength in the horizontal x and y directions, respectively.

For equal divergences with perfect parameters and a ± 4% change in the parameters, Figs. 2 and 3 are displayed by the RS frequency. From the graphical representation, it can be observed that the RS of ethanol, butanol, and propanol decreases from 1.10 THz to 3 THz due to frequency diversity, and it behaves like an additional accumulative mode from 1.0 THz to 0.8 THz. The numerical data associated with Ethanol, Butanol, and Propanol, where their respective refractive indices are 1.354, 1.3993, and 1.384, and the comparatively sensitive values for them are 91.35%, 92.55%, and 90.40%, respectively.

Figure 4 depicted the EMI for the two contrasting views of the optimal layout. The attempts to raise the EMI by repetition increase are seen. With 0.8 THz of repetition, the highest EMI begin estimating at 1.26, while the maximum repeating value with the most giant crest approximate is achieved at 3 THz with a value of 1.40. At a frequency of 1 THz, the refractive indices of Ethanol, Butanol, and Propanol are respectively each have EMI standards of 1.26, 1.32, and 1.31.

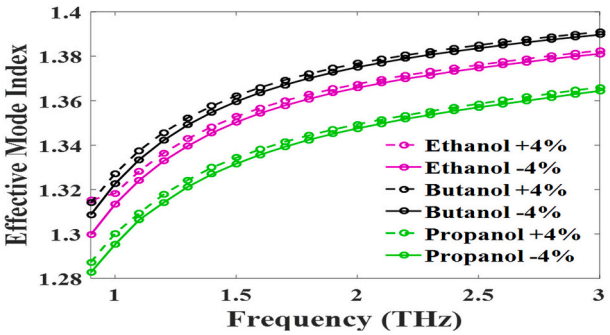

Fig. 5. EMI pertaining to three chemical frequencies with ±2% variations with the ideal parameters for both polarizations.

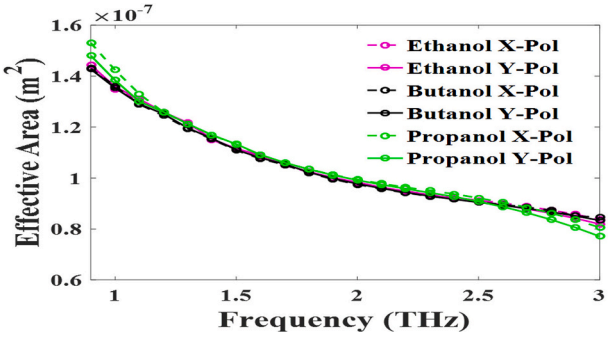

Fig. 6. EA with various frequencies.

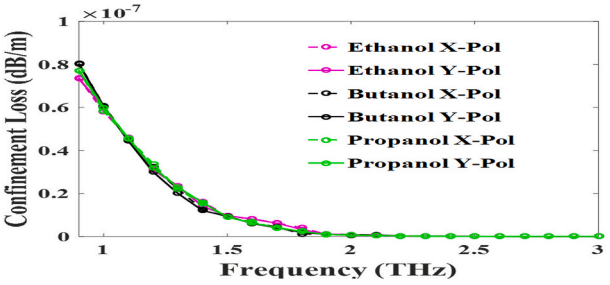

Fig. 7. Confinement loss and various frequencies are shown to help with design parameter optimization.

Figure 5 contrasts recurrence with the perfect timetable for ±4% of the types. It was observed that the expansion of the repetition waves with the EMI. In this instance, EMI exhibits the initial high value of 1.27 at a frequency of 0.8 THz, and an exceptional peak value of 1.40 at a frequency of 3 THz.

The optical portion of any PCF fiber is referred to as effective area (EA). We also see strong RS and low CL in the bigger EA-PCF. Thus, the determination of the effective area, also known as (EA) was successfully concluded [20].

$$A_{eff} = \frac{\left[\int I(rt)rtdrt\right]^2}{\left[\int I^2(rt)drt\right]^2}, \left(m^2\right) \tag{3}$$

The effective area (EA) depicted in Fig. 6 accepts the hexahedron PCF's repetition for better building is depicted. In this instance, the reduction in effective area (EA) corresponds to an increase in the frequency range from 0.8 to 3 THz. In the 1 THz operating region, the effective area (EA) values for Ethanol, Butanol, and Propanol are 1.38×10^{-7}, 1.75×10^{-7} m^2 and 1.39×10^{-7} m^2.

Another optical loss typical of the PCF architecture is confinement

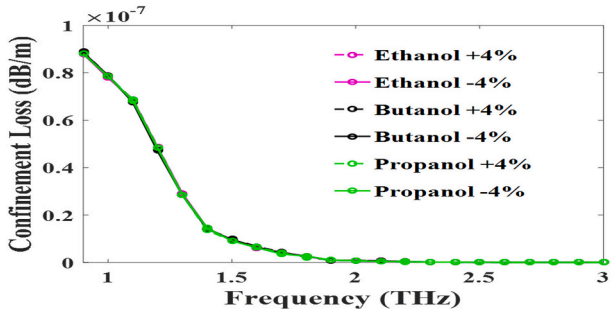

Fig. 8. Confinement loss along and various frequencies at ±4 Variations.

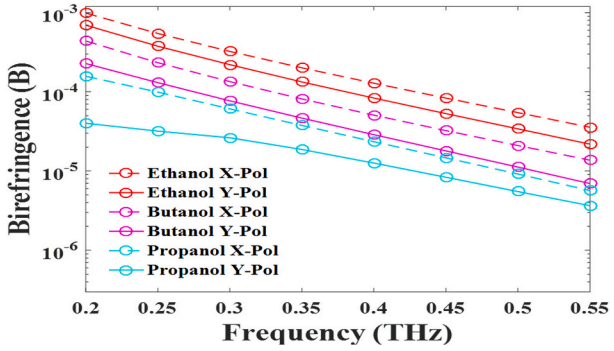

Fig. 9. To achieve the best design, the birefringence of created PCF is estimated at different frequencies.

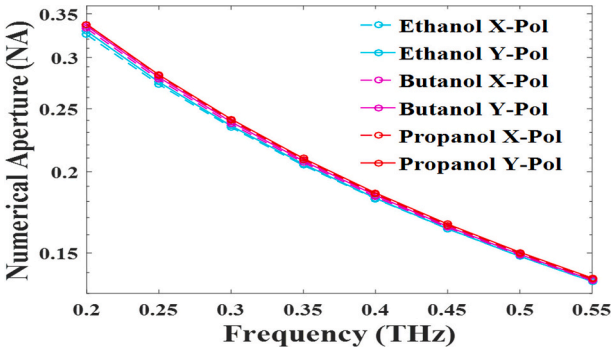

Fig. 10. For the best design considerations, NA together with a range of frequencies.

loss. The in-height RS is also visible on the low CL-PCF. The expression containment loss was assessed in this instance [21]:

$$L_c = 8.686 \times K_0 \, Im \left[n_{eff}\right] \, (dB/m) \tag{4}$$

Here, $K_0 = 2\pi\left(\frac{f}{c}\right)$, the speed of photon is c and the frequency is f. Besides, the effective mode index as an imaginary part is $I_m(n_{eff})$.

Figure 7 displays the confinement loss (CL) responses with variations in frequency within the ideal plan. To enable the recurrent wave to beat to increase, the CL drops. It was also demonstrated that the CLs are still in competition between 2.10 and 3 THz. At a frequency of 1 THz, the impact of confinement on ethanol, butanol and propanol are correspondingly (n = 1.354, 1.3993 and 1.384) results in attenuation coefficients of 5.44×10^{-08} dB/m, 6.75×10^{-08} dB/m, and 5.85×10^{-08} dB/m, respectively. We can see that the CL's disparities are significantly less significant than the ideal business constraints for graphic results.

According to Fig. 8, confinement losses (CL) for varieties with a ± 4% growth rate are equivalent to a recurrence with perfect plan

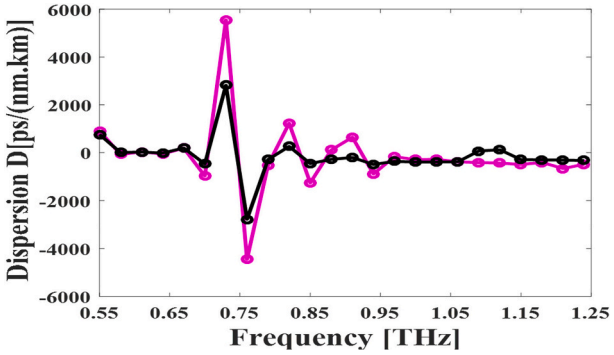

Fig. 11. For optimal shape, the spread of the intended HX-PCF is estimated at different frequencies.

constraints. The CL is reduced in line with the improvement in repeatability of the figure. The repetition between 2.10 THz and 3 THz demonstrates CL's continued dependability. (See Figs. 9 and 10.)

Birefringence occurs if there is any asymmetry in the core-clad shapes, and it may be calculated as shown below [22]:

$$B = |nx - ny| \tag{5}$$

The numerical aperture (NA) of an optical fiber is a measure of its light-gathering capacity and determines the acceptance angle of light entering the fiber. It is defined as the sine of the half-angle of the maximum cone of light that can enter the fiber and propagate down its length. The NA is typically denoted by the symbol "NA" and is dimensionless. The numerical aperture (NA) will change depending on RI variation which is stated as [23]:

$$\mathrm{NA}\ (\mathrm{R}, \alpha) = \sqrt{n_{core}^2 - n_{cladding}^2 \left(\frac{R + r}{\mathrm{R} + \alpha}\right)^2} \tag{6}$$

where n_{core} and $n_{cladding}$ are the refractive indexes, RI of the fiber core and cladding, respectively, while R stands for the radius of curvature, r for the radius of the fiber core, and α for the acceptance angle of the fiber.

The NA of an optical fiber is determined by the refractive indices of the core and cladding materials surrounding it. The core is the central region through which light travels, while the cladding is the outer layer that surrounds the core, designed to contain, and guide the light within the fiber.

Dispersion in optical fiber refers to the spreading or broadening of optical signals as they propagate through the fiber. This phenomenon arises due to the different propagation speeds of different wavelengths of light, causing the pulses to spread out over distance and time. The dispersion profile is directly impacted by the PCF's ERI. The value of β, which is modality propagation constant, is derivable by means of the Taylor expansion in second order, as illustrated in [24]:

$$\beta_2 = \frac{2}{c}\frac{dn_{eff}}{d\omega} + \frac{\omega}{c}\frac{d^2 n_{eff}}{d\omega^2}, [\mathrm{ps/THz/cm}] \tag{7}$$

The propagation mode has two polarizations (x and y polarizations), $N_{eff} = \mathrm{Re}\ (\beta)\omega/c$ and $\omega = 2\pi f$. The two polarizations that are utilized in the x and y propagation modes. In Fig. 11, it showed how to apply equations. The close-fitting behavior of polarization curves on both exerting left and right, they turned themselves is nicely shown in Fig. 11. In a wider frequency band, an even distribution between 0.97 THz and 1.09 THz that is nearly nil has been observed.

Sometimes, it is feasible to simultaneously transmit several optical signals with similar pulse spreads. The transmitted optical signal's bandwidth can be increased thanks to the lower dispersion value. A flattened dispersion around zero is also seen over a more comprehensive frequency range of 0.97 THz to 1.09 THz. On certain occasions, it is possible for multiple optical signals to be transmitted at the same time, with their pulse spread being almost identical. The transmitted optical signal's bandwidth can be increased thanks to the lower dispersion value. The proposed fiber exhibits this behavior with optical parameters, which is advantageous.

The optimal design and designs for optical options like the RS and CL of the Q-PCF have both demonstrated contrasts of around ±4%. Table 1 demonstrates the ±4% variations' modest sum of significant differences, and the RS and CL are best for unwinding. Thus, to avoid the manufacturer's intricacy, we use superior plans. We are therefore prepared to state unequivocally that the suggested Q-PCF configuration is considered more suitable for industrial or biomedical applications, considering the positioning of the chemicals is involved.

Finally, Table 2 demonstrates that the recommended optical sensor based on quasi-shaped spectroscopy has a greater PCF than the other PCFs. As a result, when the PCF is placed, it will be crucial in optical waveguides as well as optical devices.

Here, Q-PCF framework's innovative approach is a crucial element. The most popular construction techniques, including passenger plug, sol-gel, tiresome, attraction, and stack, are currently used to create PCFs. Recently, the method of Sol-gel [32,33] has been investigated as a means of improving sensor PCFs. However, this specific filling technique [34,35] leads to the center zones' filling of chemicals or in any stack containing PCF fibers. Superior management characteristics like RS, accidents, EA, TPF, and EMI are improved because of choosing the feasible investigation on this particular supplemental method.

4. Conclusion

Our idea involves employing fibers with hexahedron cores and Quasi shape cladding for alcohol and sensory monitoring. Here, we designed this fiber using the perfectly matched layer (PML) as well as COMSOL software that is based on the finite element approach to get all the numerical sensitivity of about 91.35%, 92.55%, and 90.40%and low confinement losses (CLs) of 5.44×10^{-08}, 6.75×10^{-08} dB/m, and 5.85×10^{-08} dB/m for detecting alcohols like ethanol ($n = 1.354$), butanol ($n = 1.3993$), and propanol($n = 1.384$), at 1 THz. The suggested sensor is believed to have an enhanced geometrical structure that is production friendly, enabling it to be used in practical settings like industry and biological medicine.

Funding

To conduct this research, the authors received no support.

Author statement

All authors agreed to submit the paper to this journal. The new authors have performed works to revised the manuscript.

Table 1
The table displays the best values around 1 THz with ±4% variations.

Parameters (%)	Relative sensitivity (%)			Confinement loss (dB/m)		
	Ethanol	Butanol	Proponal	Ethanol	Butanol	Propanol
+ 4%	92.27	93.53	91.22	7.05×10^{-08}	7.96×10^{-08}	7.65×10^{-08}
Optimum	91.35	92.55	90.40	5.44×10^{-08}	6.75×10^{-08}	5.85×10^{-08}
−4%	90.50	91.45	89.25	7.40×10^{-08}	7.70×10^{-08}	7.90×10^{-08}

Table 2
The comparison table compares the optical characteristics of the Q-PCF structure to those of other PCFs.

Prior in PCFs	Operating region	Relative Sensitivity (%)	Confinement loss (dB/m)	Design of structure	
				Core	Cladding
PCF_1 [25]	f = 1 THz	60.05	1.43×10^{-11}	Rotated-Hexa circular holes	Heptagonal
PCF_1 [26]	f = 1.2 THz	64.00	1.12×10^{-11}	Elliptical holes	Quasi
PCF_1 [27]	f = 1 THz	74.54	7.72×10^{-08}	slotted core	Quasi
PCF_1 [28]	f = 1.3 THz	78.80	2.19×10^{-09}	Elliptical holes	Quasi
PCF_1 [29]	f = 1 THz	45.13	5.583×10^{-05}	Circular holes	Hexagonal
PCF_1 [30]	f = 1 THz	55.56	1.00	Rhombic holes	Hexagonal
PCF_1 [31]	f = 1 THz	80.93	1.23×10^{-11}	Elliptical hole	Circular
Proposed Q -PCF	f = 1 THz	91.35	5.44×10^{-08}	Hexahedron	Quasi

CRediT authorship contribution statement

Md. Selim Hossain: Conceptualization, Methodology, Formal analysis, Writing – original draft. **Rakib Hossen:** Methodology, Formal analysis. **Shuvo Sen:** Conceptualization, Writing – original draft.

Declaration of Competing Interest

The authors declare that they have no conflict of interest.

Data availability

This research has enough data that was obtained from the simulation work using the COMSOL Multiphysics software.

Acknowledgement

The people who participated in this study are appreciated by the authors. For this study, the writers were not financially supported.

References

[1] Farhana Akter Mou, Md. Moshiur Rahman, Mohammad Rakibul Islam, Mohammed Imamul Hassan Bhuiyan, Development of a photonic crystal fiber for THz wave guidance and environmental pollutants detection, Sensi. Bio-Sens. Res. 29 (2020) 100346. ISSN 2214-1804, https://doi.org/10.1016/j.sbsr.2020.100346.
[2] E.R. Vera, J.U. Restrepo, C.J. Durango, J.M. Cardona, N.G. Cardona, Design of low loss and highly birefringent porous core photonic crystal fiber and its application to terahertz polarization beam splitter, IEEE Photonic J. vol. 10 (4) (2018).
[3] L. Ho, M. Pepper, P. Taday, Terahertz spectroscopy: signatures and fingerprints, Nat. Photonics 2 (9) (2008) 541.
[4] S. Rana, A.S. Rakin, M.R. Hasan, M.S. Reza, R. Leonhardt, Low loss and flat dispersion Kagome photonic crystal fiber in the terahertz regime, Opt. Commun. 410 (2018) 452–456.
[5] S. Asaduzzaman, K. Ahmed, T. Bhuiyan, T. Farah, Hybrid photonic crystal fiber in chemical sensing, Springer Plus 5 (1) (2016) 748.
[6] M.F.H. Arif, M.J.H. Biddut, Enhancement of relative sensitivity of photonic crystal fiber with high birefringence and low confinement loss, Optik-Intern. J. Light Elect. Optics 131 (2017) 697–704.
[7] K. Ahmed, B.K. Paul, S. Chowdhury, S. Sen, M.I. Islam, M.S. Islam, M.R. Hasan, S. Asaduzzaman, Design of a single-mode photonic crystal fibre with ultra-low material loss and large effective mode area in THz regime, IET Optoelectron. 11 (2017) 265–271.
[8] H. Ademgil, S. Haxha, PCF based sensor with high sensitivity, high birefringence and low confinement losses for liquid analyte sensing applications, Sensors 15 (12) (2015) 31833–31842.
[9] H. Ilatikhameneh, T. Ameen, F. Chen, H. Sahasrabudhe, G. Klimeck, R. Rahman, Dramatic impact of dimensionality on the electrostatics of P-N junctions and its sensing and switching applications, IEEE Trans. Nanotechnol. (2018), https://doi.org/10.1109/TNANO.2018.2799960.
[16] Md. Abdullah-Al-Shafi, Nasima Akter, Md. Shuvo Sen, Selim Hossain, Design and performance analysis of background material of zeonex based high core power fraction and extremely low effective material loss of photonic crystal fiber in the terahertz (THz) wave pulse for many types of communication areas, Optik 243 (2021) 167519. ISSN 0030-4026,, https://doi.org/10.1016/j.ijleo.2021.167519.
[18] M.S. Islam, J. Sultana, M. Dorraki, J. Atai, M.R. Islam, A. Dinovitser, D. Abbott, Low loss and low dispersion hybrid core photonic crystal fiber for terahertz propagation, Photon Netw. Commun. 35 (3) (2018) 364–373.
[19] M.S. Hossain, A.S. Sikder, S. Sen, et al., Design and numerical analysis of Zeonex-based photonic crystal fiber for application in different types of communication networks, J. Comput. Electron. 20 (2021) 1289–1295, https://doi.org/10.1007/s10825-021-01704-9.
[21] G.K.M. Hasanuzzaman, M.S. Habib, S.A. Razzak, M.A. Hossain, Y. Namihira, Low loss single-mode porous-core kagome photonic crystal fiber for THz wave guidance, J. Lightwave Technol. 33 (19) (2015) 4027–4031.
[22] M.M. Rahman, F.A. Mou, M.I.H. Bhuiyan, M.R. Islam, Extremely low effective material loss of air core photonic crystal Fiber for THz guidance, in: IEEE Region 10 Symposium (TENSYMP), Kolkata, India, 2019, pp. 716–720, https://doi.org/10.1109/TENSYMP46218.2019.8971297(2019).
[23] R.K. Gangwar, V.K. Singh, Study of highly birefringence dispersion shifted photonic crystal fiber with asymmetrical cladding, Optic 127 (24) (2016) 11854–11859.
[24] M.R. Hasan, S. Akter, T. Khatun, A.A. Rifat, M.S. Anower, Dual-hole unit-based kagome lattice microstructure fiber for low-loss and highly birefringent terahertz guidance, Opt. Eng. 56 (4) (2017), 043108.
[25] M.R. Hasan, M.A. Islam, A.A. Rifat, A single mode porous-core square lattice photonic crystal fiber for THz wave propagation, J. Eur. Opt. Soc. Rapid. Publ. 12 (1) (2016) 15, https://doi.org/10.1186/s41476-016-0017-5.
[26] K. Ahmed, S. Chowdhury, B.K. Paul, M.S. Islam, S. Sen, M.I. Islam, Ultrahigh birefringence, ultralow material loss porous core single-mode fiber for terahertz wave guidance, Appl. Opt. 56 (12) (2017) 3477–3483, https://doi.org/10.1364/AO.56.003477.
[27] S. Rana, G.K. Hasanuzzaman, S. Habib, S.F. Kaijage, R. Islam, Proposal for a low loss porous core octagonal photonic crystal fiber for T-ray wave guiding, Opt. Eng. 53 (11) (2014) 115107, https://doi.org/10.1117/1.OE.53.11.115107.
[28] Md Saiful Islam, J. Sultana, K. Ahmed, M. Rakibul Islam, A. Dinovitser, B. Wai-Him Ng, D. Abbott, A novel approach for spectroscopic chemical identification using photonic crystal fiber in the terahertz regime, IEEE Sensors J. 18 (2018) 575–582.
[29] Md Saiful Islam, J. Sultana, A.A. Rifat, A. Dinovitser, B. Wai-Him Ng, D. Abbott, Terahertz sensing in a hollow core photonic crystal fiber, IEEE Sensors J. 18 (2018) 4073–4080.
[30] M.R. Hasan, M.A. Islam, M.S. Anower, S.M. Razzak, Low-loss and bend-insensitive terahertz fiber using a rhombic-shaped core, Appl. Opt. 55 (30) (2016) 8441–8447, https://doi.org/10.1364/AO.55.008441.
[31] G.K.M. Hasanuzzaman, S. Rana, M.S. Habib, A novel low loss, highly birefringent photonic crystal Fiber in THz regime, IEEE Photon. Technol. Lett. 28 (April 8) (2016) 899–902.
[32] Y.S. Lee, C.G. Lee, Y. Jung, M.K. Oh, S. Kim, Highly Birefringent and dispersion compensating photonic crystal fiber based on double line defect core, J. Opt. Soc. Korea 20 (5) (2016) 567–574.
[33] M.S. Hossain, S. Shuvo, M.M. Hossain, Design of a chemical sensing circular photonic crystal fiber with high relative sensitivity and low confinement loss for terahertz (THz) regime, Optik - Intern. J. Light Elect. Optics 222 (2020), 165359, https://doi.org/10.1016/j.ijleo.2020.165359(2020).
[34] R. Islam, S. Rana, R. Ahmad, S.F. Kaijage, Bend-insensitive and low-loss porous Core spiral terahertz Fiber, IEEE Photon. Technol. Lett. 27 (21) (2015) 2242–2245, https://doi.org/10.1109/LPT.2015.2457941.
[35] M.R. Hasan, M.A. Islam, M.S. Anower, S.M.A. Razzak, Low-loss and bend-insensitive terahertz fiber using a rhombic-shaped core, Appl. Opt. 55 (2016) 8441–8447.